J. Biochem. **142,** 325–333 (2007)
doi:10.1093/jb/mvm135

Structural Change of Bacteriorhodopsin in the Purple Membrane above pH 10 Decreases Heterogeneity of the Irreversible Photobleaching Components

Yasunori Yokoyama[1,*], Masashi Sonoyama[1], Tatsuhiko Nakano[2] and Shigeki Mitaku[1]

[1]Department of Applied Physics, Graduate School of Engineering, Nagoya University, Furo-cho, Chikusa-ku, Nagoya, Aichi 464-8603, Japan; and [2]Scientific Instruments Division, Thermo Fisher Scientific K.K., C-2F, 3-9 Moriya-cho, Kanagawa-ku, Yokohama, Kanagawa 221-0022, Japan

published online July 23, 2007

Kinetic investigations of irreversible photobleaching of bacteriorhodopsin (bR) in purple membrane (PM) at high temperature have previously shown two kinds of bR species upon light illumination. The bR species consist of kinetically fast- and slow-denatured components, whose proportions were dependent upon structural changes in dark, as shown by CD. In order to elucidate electrostatic contribution on the heterogeneous stability and the bR structure in PM, photobleaching behaviour and structural changes over a wide pH range were investigated by kinetics as well as various spectroscopic techniques. Kinetics revealed that photobleaching below pH 9 obeyed double-exponential functions, whereas measurements above pH 10 were characterized by a single-decay component. FT-IR deconvoluted spectra showed a α_{II}-to-α_{I} transition in the transmembrane helices around pH 10. Near-IR Raman scattering spectra demonstrated the equilibrium shift of retinal isomers from all *trans* to 13-*cis* form. Near-UV CD spectra suggested configurational changes in the aromatic residues around the retinal pocket. An exciton-to-positive transition in visible CD spectrum was observed. This indicates disorganization in the 2D-crystalline lattice of PM, which occurred concomitantly with the changes above pH 10. A model for the changes in kinetic behaviour and molecular structure around pH 10 is discussed, focusing on changes in charge distribution upon alkalinization.

Key words: denaturation kinetics, intermolecular interaction, irreversible photobleaching, retinal chromophore, transmembrane helix.

Abbreviations: bR, bacteriorhodopsin; PM, purple membrane; PRG, proton release group; 2D, two-dimensional.

Bacteriorhodopsin (bR), a light-driven proton pump of *Halobacterium salinarum*, (*1*) is known to spontaneously form a 2D-crystalline array of hexagonally oriented bR trimers in the plasma membrane. The membrane patch comprised of this array is referred to as purple membrane (PM) (*2*). It is well known that proton translocation across the membrane is achieved through the photocycle, which consists of several spectrally distinguishable photo-intermediates (*3*). The intermediates are formed upon absorption of visible light by a retinal chromophore covalently bound to the protein via a Schiff base linkage (*3*). The molecular structure of the ground state of bR resolved at atomic resolution (*4–6*) shows that a number of charged amino acid residues, which act as proton donors or acceptors (*7–10*), are oriented toward each other. These amino acids form a proton channel, which involves a network of hydrogen bonds formed by water molecules inside a bundle of transmembrane helices. These charged amino acid residues contribute to function as well as structural stability because of the polar interactions inside the helix bundle (*11*, *12*). Recently, the molecular structures of several photo-intermediate (*13–15*) have been resolved, suggesting a mechanism of vectorial proton translocation.

Although the photo-intermediates of bR can return to the ground state without relaxing into denatured states under physiological conditions, irreversible photobleaching has been reported for bRs in PM at high temperature (*16–19*) and alkaline pH, (*17*, *20*) as well as in detergent micelles (*21*, *22*). The dependency of the light intensity on the photobleaching was reported for the bR in PM at high temperature (*17*). This is thought to be a result of a photoreaction of bR. Interestingly, the kinetics of the irreversible photobleaching of bR in PM at neutral pH (*19*) shows two types of bR species with respect to structural stability. This heterogeneous stability to photobleaching is influenced by structural changes in the dark, (*19*) involving secondary structure, (*23*) retinal isomerization, (*24*) disorganization of the 2D crystal (*18*, *19*) and an increase of water accessibility to the Schiff base (*25*). On the other hand, bRs solubilized by the mild non-ionic detergents, such as octyl-β-glucoside and Triton X-100, undergo irreversible photobleaching, even at around room temperature with a single-decay

*To whom correspondence should be addressed. Tel: +81-52-789-4465, Fax: +81-52-789-4465, E-mail: yokoyama@nuap.nagoya-u.ac.jp

component (*21*, *22*). The photobleaching kinetics under these conditions differ significantly, despite the similarities in the structural properties described earlier (*23*, *24*, *26*). The photocycle is maintained by the force balance between the intra- and inter-molecular interactions in bR; therefore, these structural changes are thought to be associated with the mechanisms of irreversible photobleaching. However, the specific part of the molecule essential to restoring the ground state, and what factors relate to its heterogeneous stability during the photocycle remain unknown.

In order to address these issues, the photobleaching behaviours and the structural changes of bR at high pH were investigated and compared with other photobleaching conditions. A calorimetric study for bR in PM (*27*) strongly suggested that the balance between the intra- and inter-molecular interactions in bR are effectively altered by changing the pH of the surrounding medium. Herein, two types of experiments were conducted in order to elucidate more information on the irreversible photobleaching of bR in PM at alkaline pH: (i) kinetics investigations of the irreversible photobleaching and (ii) spectroscopic measurements of bR in the dark by vibrational and circular dichroism (CD) spectroscopies. A model for the structural changes at high pH is discussed on the basis of the pK_as of the charged amino acid residues.

MATERIALS AND METHODS

Sample Preparation—PM of *H. salinarum*, strain R1M1, was purified according to standard methods (*28*). The concentration of the purified PM suspension was determined from the absorption maximum at 568 nm using an extinction coefficient of $62700 \pm 700\,M^{-1}\,cm^{-1}$ (*29*). PM suspensions of known-bR concentrations were resuspended in the following buffers for spectroscopic measurements at room temperature: 20 mM MES-NaOH (pH 6.0), 20 mM Tris-HCl (pH 7.0), 20 mM Tricine-NaOH (pH 8.0), 20 mM CHES-NaOH (pH 9.0), 20 mM CAPSO-NaOH (pH 10.0), 20 mM CAPS-NaOH (pH 11.0) and 20 mM phosphate-NaOH (pH 12.0). The pH values of the buffers were adjusted at room temperature by titrating with 1 N HCl or 1 N NaOH solutions. PM suspensions for temperature-jump experiments were also resuspended in buffers with pHs adjusted at high temperature. PM suspensions at each pH were stored in the refrigerator in the dark in order to prevent light adaptation of the samples.

Kinetics Measurements of Photobleaching—The kinetics measurements of the photobleaching of bR in PM were conducted using temperature-jump experiments under illumination with visible light during high temperatures (40–70°C) and alkaline pH (pH 7–11). The experimental setup for the temperature-jump experiments was previously described (*18*, *19*). In these experiments, absorption spectra before the temperature jump and after quenching following high-temperature incubation (10 min to 4 h) were used in order to determine reversible and irreversible components. The net kinetics curves of the photobleaching were obtained by plotting the reversible components as a function of incubation time.

Spectroscopic Measurements—Infrared (IR) spectra of the dark-adapted bR were recorded using an FTS-6000 FT-IR spectrometer (Varian Inc. Scientific Instruments, USA) equipped with an MCT detector at room temperature. PM suspensions at a bR concentration of about 1 mM were placed between two BaF_2 windows with a 6 μm PET spacer film. The spectral resolution was $2\,cm^{-1}$ and 2,048 scans were averaged for each spectrum. IR spectra of the buffer solution, recorded under the same conditions as the PM suspension, were used to subtract the spectral background using the water band at $2{,}130\,cm^{-1}$ as the criterion for the subtraction. Fourier self-deconvolution of the IR spectra was conducted according to the method established by Kauppinen *et al*. (*30*) A narrowing factor (*k* factor) of 2.5 and a bandwidth of $14\,cm^{-1}$ were used for the calculations, as previously reported (*31*).

Non-resonant near-IR Raman scattering spectra of the dark-adapted bR were collected by a Nicolet™ 6700 FT-IR equipped with a FT-Raman module (Scientific Instruments Division, Thermo Fisher Scientific Inc.) at room temperature. A diode laser (excitation wavelength: 1,064 nm) with an averaged power of about 400 mW was used as the excitation light source. PM suspensions with bR concentrations of about 1 mM were incorporated into a glass sample tube (5 mm in diameter) and 180° backscattered Raman light was collected using an InGaAs detector operating at room temperature. The spectral resolution was $4\,cm^{-1}$ and four sets of 1,024 scans were recorded and averaged for each spectrum. Curve fitting of the C=C stretching region in the Raman spectra was carried out on GRAMS/AI™ software (Informatics Division, Thermo Fisher Scientific Inc.) using the previously reported fitting parameters (*32*, *33*) as the initial values, after interpolating the spectral data with a spectral resolution of $2\,cm^{-1}$.

CD spectra of the dark-adapted bR at the near-UV and visible regions were recorded on a J-820 spectropolarimeter (Jasco Corporation, Japan) with a cylindrical quartz cell (path length of 5 mm) at room temperature. Scan speeds were 50 and $100\,nm\,min^{-1}$ and data acquisition times were 2 and 1 s for the near-UV and visible regions, respectively. The protein concentration for CD measurements was about 10 μM, and 8 scans were averaged for each spectrum. Smoothing of the visible CD spectra was performed by using a fast Fourier transform (FFT) algorithm.

RESULTS

Photobleaching Kinetics of bR in PM at Alkaline pH—In order to elucidate the photobleaching behaviours of bR in PM at high pH, the net kinetics curves of the irreversible photobleaching were measured under illumination with visible light in temperature-jump experiments. Figure 1 shows the decay curves due to irreversible photobleaching incubated at 50°C and at pHs ranging from 7.0 to 11.0. In Fig. 1, the fractions of native bR, that were recovered upon quenching following high-temperature incubation under illumination, were plotted as a function of incubation time. The decay curves for photobleaching below pH 9 exhibited two

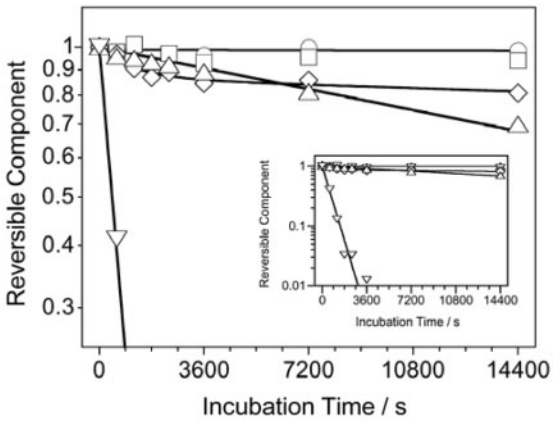

Fig. 1. **Denaturation curves of irreversible photobleaching of bR in PM incubated at 50°C at pH 7.0 (open circle), pH 8.0 (open square), pH 9.0 (open diamond), pH 10.0 (open triangle) and pH 11.0 (open-inverted triangle).** The inset is re-drawn with a wider scale of a vertical axis to show all the data at pH 11.0.

decay constants, similar to those for bR in PM at pH 7, (*19*) suggesting heterogeneous stability of bR in PM against illumination. The decay curves above pH 10, on the other hand, were in good agreement with a single-exponential function, suggesting homogeneous stability. Moreover, the irreversible photobleaching of bR with a single-decay component occurred even at around room temperature above pH 11, demonstrating a significant decrease of structural stability at high pH (data not shown). These findings strongly suggest that the distribution of bR molecules with different stabilities in PM change around pH 10. The photobleaching kinetics were biphasic at neutral pH, and monophasic at alkaline pH at temperatures in the range between 40 and 80°C.

Structural Changes of Dark-adapted bR in PM at Alkaline pH—We previously reported (*18*, *19*, *26*) that heterogeneity during photobleaching is related to the structural changes of bR in the dark. Therefore, the structural changes of dark-adapted bR in PM were investigated upon alkalinization using a variety of spectroscopic techniques. Changes in the secondary structure were investigated using IR spectroscopy. Figure 2(A) shows the amide I and II regions of the FT-IR spectra of PMs at pHs ranging from 6.0 to 12.0. The IR spectra of the PM suspension at netural pH showed little variation from previous results (*26*, *31*, *34*, *35*). Figure 2(A) shows that the amide I band starts to undergo a downshift from 1,663 to 1,660 cm^{-1} at pH 10, whereas little bandshift is observed for the amide II region, even at extremely high pHs. In order to elucidate information about the secondary structure, spectral deconvolution of the amide I band was carried out (Fig. 2B). Two major maxima in the amide I region were observed at 1,658 and 1,665 cm^{-1}. The centre position of the shoulder peak at 1,658 cm^{-1} was read by using the second derivative analysis for the original IR spectra. The band observed at 1,658 cm^{-1} is in good agreement with the position of the standard α-helix (referred to as α_I) (*36–40*). Krimm and Dwivedi (*36*) proposed that the higher frequency band at 1,665 cm^{-1} could be attributed to a helical structure in which hydrogen bonds in the peptide backbone are slightly elongated and tilted toward the helix axis (referred to as α_{II}), thus resulting in a slight weakening of the hydrogen bond. Figure 2B shows that the peak intensity of the 1,665 cm^{-1} band began to decrease at pH 10. This decrease was observed concomitant with an increase of the band at 1,658 cm^{-1}. Figure 2(C) shows the pH dependence of the peak intensity ratio of 1,658 cm^{-1} to 1,665 cm^{-1} from the deconvoluted spectra shown in Fig. 2(B). The peak intensity ratio of the two bands was almost identical up to pH 9, and then increased abruptly above pH 10. This result indicates that a change in the secondary structure, from α_{II} to α_I in bR in PM, occurred in this pH range.

The isomerization of the retinal chromophore of the dark-adapted bR was investigated with non-resonant near-IR Raman spectroscopy. In this work, '*in situ*' Raman spectroscopic measurement was operated in order to avoid the unanticipated changes in the chromophore due to the extraction for the HPLC analysis in the extremely high pH condition. Figure 3(A) shows FT-Raman spectra of bR in PM over the same pH range. The spectra measured at neutral pH were in good agreement with those previous reported, containing C=C stretching at 1,526 cm^{-1} with a shoulder at 1,534 cm^{-1}, C-C stretching at 1,199, 1,181, 1,166 cm^{-1}, CH_3 rocking band at 1,007 cm^{-1}, and the 14-hydrogen-out-of-plane (14-HOOP) mode at 798 cm^{-1} (*26*, *32*, *33*, *41*). The double peaked structure of the C=C stretching band, with maxima at 1,526 and 1,534 cm^{-1}, was assigned to the all *trans* and the 13-*cis* isomers, respectively (*42–45*). Figure 3(B) shows expanded spectra of the C=C stretching region. These spectra demonstrate that the Raman intensity of the 1,526 cm^{-1} band started to decrease, concomitant with an increase in the band at 1,534 cm^{-1} at pH 10. For quantitative determination of the retinal isomeric ratio under each condition, curve fitting against the double-peaked band with two Voigtian functions was carried out according to the method established by Schulte *et al*. (*32*) and Schulte and Bradley (*33*). The curve fitting produced very good results (dotted traces), showing the pH dependence of the retinal isomerization from the all *trans* to the 13-*cis* form. Supposing that the isomeric ratio of the two isomers in the dark-adapted bR at neutral pH was almost one (*46*), the ratio of the scattering cross-section $\sigma_{\text{all } trans}$ to $\sigma_{13\text{-}cis}$ was calculated by fitting the two peak areas. The isomeric ratios at higher pHs were subsequently estimated using this scattering cross-section ratio. Assuming that these cross-sections do not change considerably at high pH, the pH dependence of the ratio of the two isomers in the dark-adapted state was calculated from the curve fitting results (Fig. 3C). Figure 3(C) indicates that the population of the 13-*cis* form increased drastically above pH 10, and that the 13-*cis* form was the dominant isomer in the dark-adapted bR in PM at pH 12.

In order to investigate the changes in bR molecular structures in PM upon alkalinization, CD spectra of the dark-adapted bR were taken over the same pH range. Figure 4(A) shows the near-UV CD spectra of bR at

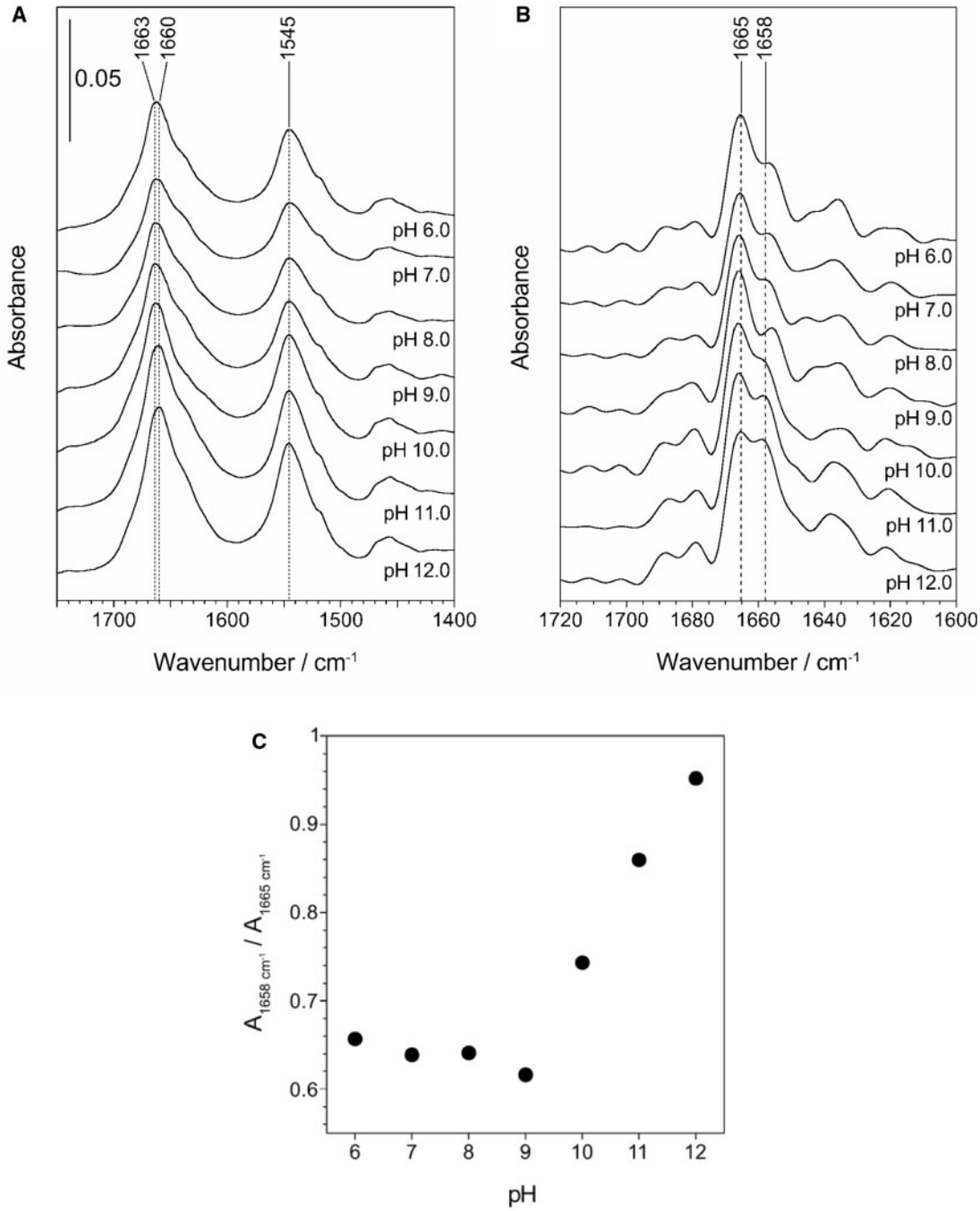

Fig. 2. **(A) FT-IR spectra of the dark-adapted bR in PM at indicated pH conditions.** (B) Deconvoluted spectra (amide I region), obtained using a narrowing factor (*k* factor) of 2.5 and a bandwidth of 14 cm^{-1}. (C) pH dependence of peak intensity ratio of 1658 cm^{-1} to 1665 cm^{-1} from the deconvoluted spectra.

each pH (upper column) and the difference spectra from the spectrum measured at pH 7.0 (lower column). Three major CD bands at 265, 290 and 320 nm were obtained at neutral pH. A decrease of the 265 and 320 nm bands and a slight increase around 280 nm were observed with an increase in pH, as previously reported (*47*). Previous works (*47*, *48*) revealed that the positive and negative bands at 265 and 320 nm were derived from the retinal chromophore, whereas a positive band around 290 nm was attributed to the side chain of the aromatic amino acid. The difference spectra clearly show that the new CD band around 280 nm appeared at pH 10, indicating a structural change around the aromatic amino acid residues of bR at high pH. The pH dependence of the change in the molar ellipticity at 280 nm is shown in Fig. 4(B). The changes in the CD at 280 nm were clearly seen above pH 10, whereas bR in PM remained in its native configuration up to pH 9.

CD spectra of the visible region were also taken to elucidate the molecular assembly in the membrane.

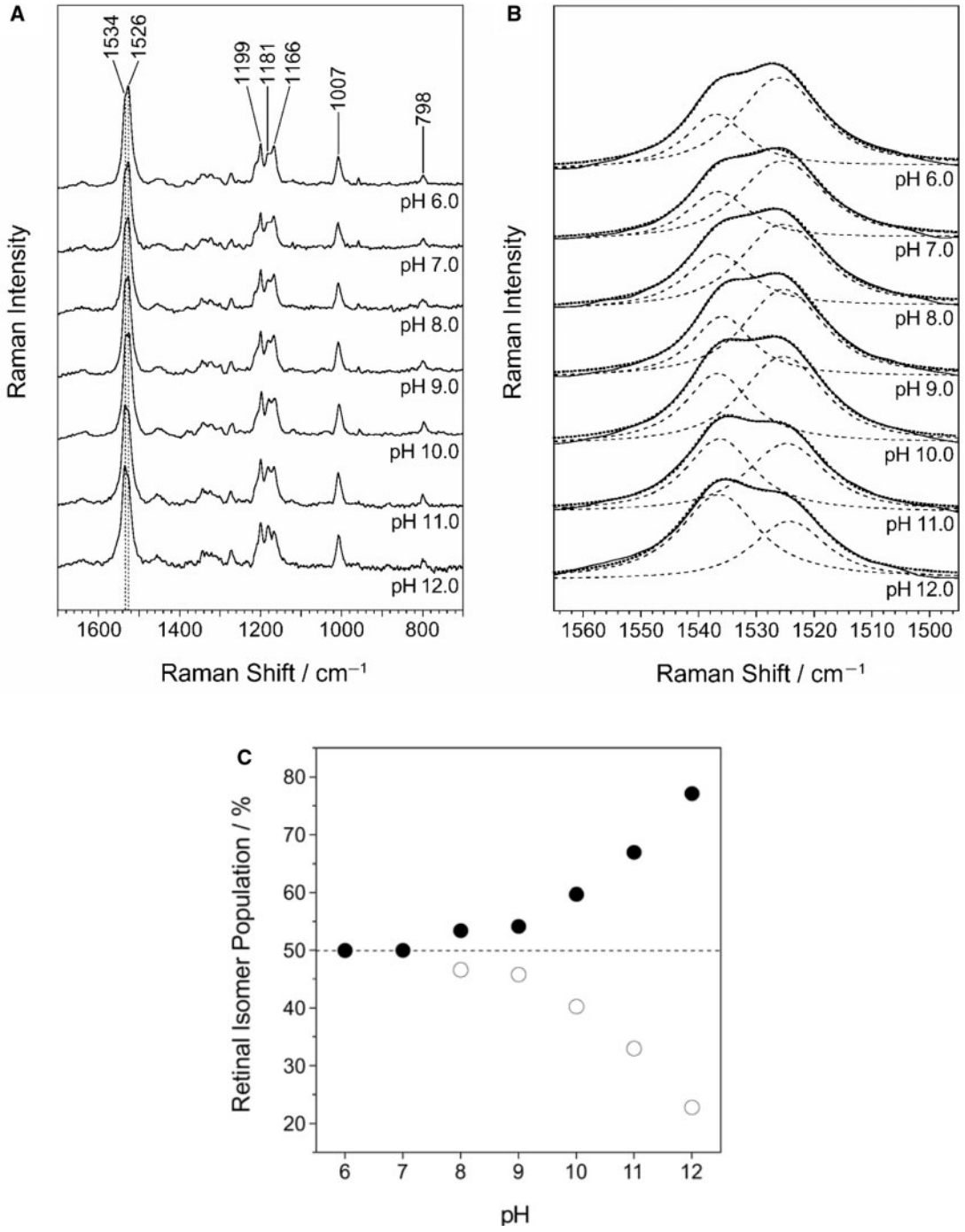

Fig. 3. **(A) FT-Raman spectra of dark-adapted bR in PM at indicated pH conditions.** (B) Curve fitting results of the C=C stretching region of Fig. 3(A); original spectra (solid lines), single Voigtian curves assigned to the all *trans* and the 13-*cis* isomers (broken lines) and the results of fitting (thick-dotted lines). (C) pH dependence of the populations of the retinal isomers obtained from the results of curve fitting shown in Fig. 3(B); all *trans* form (open circles) and 13-*cis* form (filled circles).

Figure 5(A) shows the visible CD spectra of the dark-adapted bR over the same pH range. The exciton-type CD band at neutral pH was transformed to the positive-type band with increasing pH, as previously reported (*47*). The peak intensity of both positive and negative lobes of the exciton-type CD band became weaker with increasing pH. The diminutions of these lobes of the exciton CD band were attributed to a weakening of the exciton coupling between the retinal chromophores on PM, due to disorganization of the crystalline lattice (*48–50*). Hiraki *et al*. (*49*) reported that a bilobed spectrum of the exciton-type CD band indicated a 2D-crystalline structure in PM with a trimeric bR state, whereas spectral changes to a positive-type CD band corresponded to a melting of the crystalline array. The CD intensity of the negative lobe at 600 nm was used to analyse the exciton-to-positive transition in the visible CD

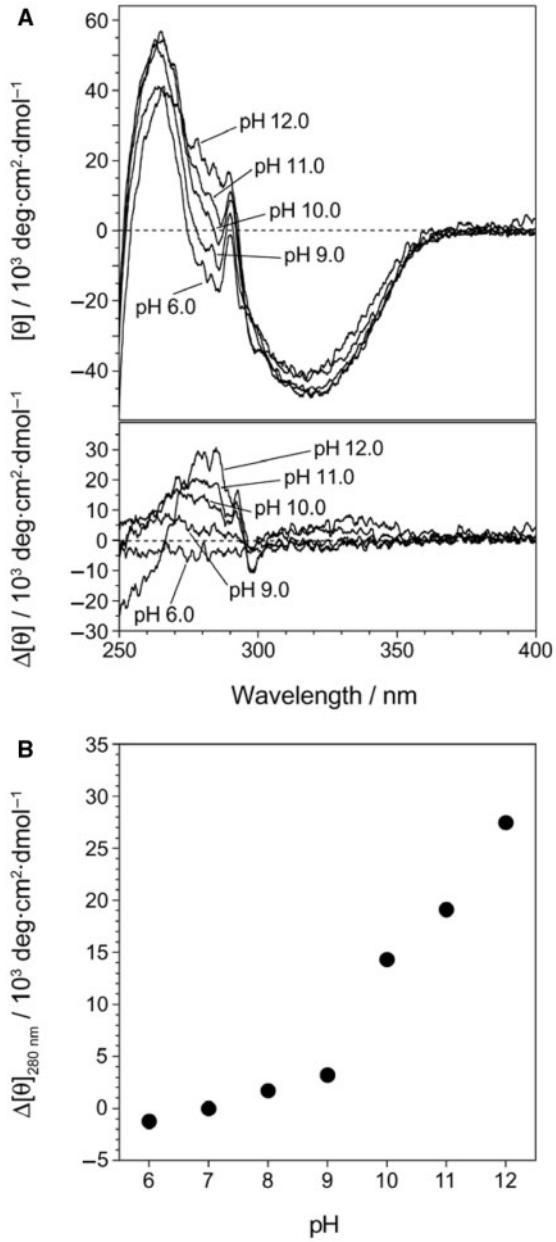

Fig. 4. **(A) Near-UV CD spectra of the dark-adapted bR in PM at indicated pH conditions (upper column), and difference spectra from the spectrum measured at pH 7.0 (lower column).** (B) pH dependence of CD intensity change at 280 nm.

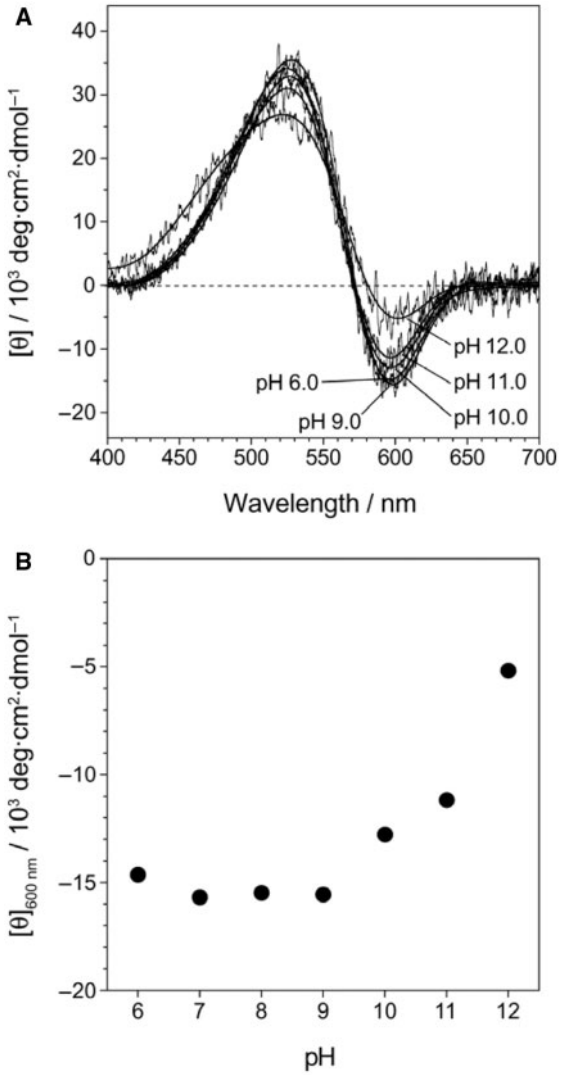

Fig. 5. **(A) Visible CD spectra of the dark-adapted bR in PM at indicated pH conditions.** Gray and solid traces indicate the spectra before and after smoothing, respectively, by using a FFT algorithm. (B) pH dependence of CD intensity at 600 nm from the smoothed spectra.

spectrum. The pH dependence of the CD intensity at 600 nm shown in Fig. 5(B) is similar to that of the secondary structure, the isomeric state of the retinal chromophore and the structures around aromatic residues (Figs. 2C, 3C and 4B).

DISCUSSION

In this study, photobleaching experiments of bR in PM at high temperature and high pH revealed not only that the temperature range of the irreversible photobleaching became lower, but also that the photobleaching kinetics drastically changed upon alkalinization. Our previous works (*18*, *19*) revealed that the irreversible photobleaching of bR in PM at high temperature occurred when its structure in the dark transformed to the non-native state and that the proportion of two decay components of the photobleaching was also dependent on the structural changes of bR in the dark. These results imply that the photobleaching phenomenon should be related with the changes in the intra- and intermolecular interactions of the dark state of bR in PM. As shown in Fig. 1, the photobleaching kinetics below pH 9 was characterized by two decay components, whereas those above pH 10 obeyed a single-exponential function. These findings strongly suggested that structural changes in the dark-adapted bR in PM occurred in this pH range. Therefore, the structural changes in bR

were investigated in the dark under a constant temperature in an effort to elucidate the effect of pH on bR structure. Results showed that four types of structural changes simultaneously occurred above pH 10: the α_{II}-to-α_I transition in the secondary structure, the local configurational changes of the aromatic residues in the tertiary structure, retinal isomerization from the all *trans* to the 13-*cis* form and disorganization of the 2D-crystalline lattice of PM. The discussion of these results will focus on two points: (i) the cause of the structural changes in bR above pH 10 and (ii) the relationship between the structural changes and the irreversible photobleaching.

The spectral changes in bR upon alkalinization observed in this work, including retinal isomerization and the configurational changes of the aromatic residues (Figs 3A and 4A) were primarily attributed to structural changes around the retinal pocket in the centre of the transmembrane region. It is not reasonable that alternation in the pH of the surrounding medium directly influences the structures around the retinal pocket. Thus, it is reasonable that another region propagates the change in the medium pH to the internal region. Therefore, we initially focused on the charged residues in the hydrophilic regions.

The proton release group (PRG) consists of a hydrogen-bonded network between Arg82, Glu194 and Glu204 at the extracellular proton channel (*6*). PRG, for which pK_a of the deprotonated form was about 9.7, (*51*) has been suggested as one of the candidates responsible for structural changes in charged residues around pH 10. Some structural changes have been reported to occur in bR due to charge distribution changes in the PRG. The mutations to the charged residues in the PRG influenced the dark-adaptation rate of the retinal, (*51–53*) a local structure around Asp85, *i.e*. in the vicinity of the Schiff base (*54*) and the water accessibility to the Schiff base in the dark (*55*). The finding that deprotonation of the Schiff base started to be observed at pH 11.5 in the dark also suggests easier accessibility of water molecules to the Schiff base (*56*). These results strongly suggest that alteration of the charge distribution in the PRG at the extracellular surface influences the internal region. On the other hand, the cytoplasmic proton channel is covered with bulky, hydrophobic amino acid sidechains (*4–6*). The charge distribution of the carboxyl groups at the cytoplasmic surface is not considered to be affected at high pH, because these residues are presumably ionized at neutral pH (*53*). This suggests that structural changes of bR observed in this work, were induced by the alternation of the charge distribution at the extracellular side. The deprotonation of the positively charged residues at the membrane interface region should also be considered to correlate with the structural changes of bR in PM at high pH. A number of the positively charged residues directly interact with the lipid molecules of PM via electrostatic interaction (*5*). Probably, the melting of the 2D-crystalline lattice was induced by the change in the intermolecular interaction involving the lipid molecules.

The relationship between the structural changes and the photobleaching behaviours must also be considered. We herein discuss this point, taking the cases of other

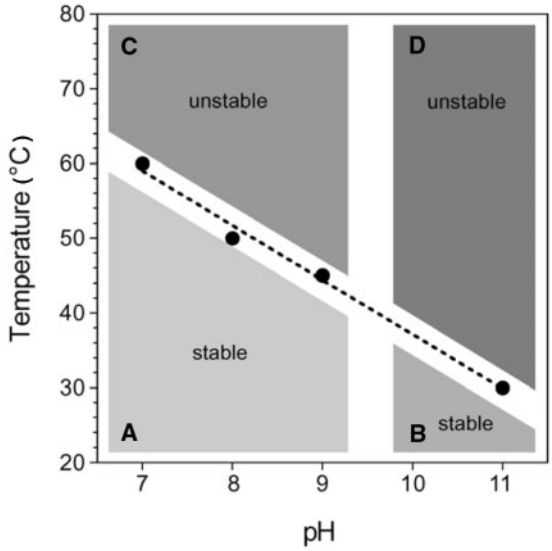

Fig. 6. **A phase diagram of the photobleaching phenomenon of bR in PM in respect of the temperature and pH.** The diagram shows the pH dependence of the onset temperature of photobleaching as well as the photobleaching behaviour (biphasic or monophasic decay) and the heterogeneity in bR species in the dark at room temperature: (A) stable photocycle, heterogeneous bR species in the dark, (B) stable photocycle, almost homogeneous bR species in the dark, (C) photobleaching with two decay componentsand (D) photobleaching with a single-decay component.

photobleaching conditions into account. The phase diagram of the photobleaching of bR in PM in respect of temperature and pH is shown in Fig. 6. In Fig. 6, a pH dependence of the onset temperature of the photobleaching was depicted as well as the number of decay component of photobleaching and the heterogeneity of bR structure in the dark at room temperature. The structural changes of bR in PM at alkaline pH observed in this work were similar to those observed at high temperatures at neutral pH for the secondary structure, (*23*) the retinal isomerization, (*24*) the melting of the 2D-crystalline lattice (*18*, *19*) and the enhancement of water accessibility to the Schiff base (*25*). These results imply that bR molecules in PM assume a structure described earlier in the disordered 2D-crystalline lattice under the photobleaching conditions independent of temperature and pH. However, although the characteristics of the bR structure are very similar, the photobleaching kinetics above pH 10 appears different.

The results of the current work were also compared with bR solubilized with octyl-β-glucoside, where irreversible photobleaching occurs at room temperature with a single-decay component (*21*). This comparison is expected to help clarify what other aspects of the bR molecule are responsible for the difference in the photobleaching kinetics. bR molecules are present as monomer units in the detergent micelles; (*57*) therefore, the intermolecular interactions between bR molecules in the lattice are lost. Furthermore, both retinal isomerization from the all *trans* to the 13-*cis* form and the α_{II}-to-α_I transition were observed upon solubilization (*26*).

This suggests that the intermolecular interaction between bR molecules in the lattice significantly influences the molecular structure. The characteristics of the molecular structure and the photobleaching kinetics are quite similar for bR in PM at alkaline pH and the solubilized bR. Thus, it is likely that the number of decay components during the irreversible photobleaching are affected by intermolecular interactions. Assuming that the intermolecular interaction is related to the distribution of the bR species in PM, most of the bR molecules assume a relaxed structure in which the intermolecular interactions are weakened. Indeed, bR in PM above pH 11 underwent irreversible photobleaching with a single-decay component, even at around room temperature. In any case, it is considered that the structure around the extracellular proton channel including the hydrogen-bonding network plays an important role for structural recovery from the photo-intermediates. It is not contradictory that the photo-intermediates in which the cytoplasmic channel is open cannot return to the ground state when the structure of the extracellular side is perturbed.

This work was supported in part by a Grant-in-aid for scientific research from the Ministry of Education, Culture, Sports, Science and Technology (Monbukagakusho) of Japan and by SENTAN, JST.

REFERENCES

1. Bogomolni, R.A., Baker, R.A., Lozier, R.H., and Stoeckenius, W. (1976) Light-driven proton translocations in *Halobacterium halobium*. *Biochim. Biophys. Acta* **440**, 68–88
2. Henderson, R. (1977) The purple membrane from *Halobacterium halobium*. *Annu. Rev. Biophys. Bioeng.* **6**, 87–109
3. Lanyi, J.K. (1993) Proton translocation mechanism and energetics in the light-driven pump bacteriorhodopsin. *Biochim. Biophys. Acta* **1183**, 241–261
4. Henderson, R., Baldwin, J.M., Ceska, T.A., Zemlin, F., Beckmann, E., and Downing, K.H. (1990) Model for the structure of bacteriorhodopsin based on high-resolution electron cryo-microscopy. *J. Mol. Biol.* **213**, 899–929
5. Mitsuoka, K., Hirai, T., Murata, K., Miyazawa, A., Kidera, A., Kimura, Y., and Fujiyoshi, Y. (1999) The structure of bacteriorhodopsin at 3.0 Å resolution based on electron crystallography: implication of the charge distribution. *J. Mol. Biol.* **286**, 861–882
6. Luecke, H., Schobert, B., Richter, H.-T., Cartailler, J.-P., and Lanyi, J.K. (1999) Structure of bacteriorhodopsin at 1.55 Å resolution. *J. Mol. Biol.* **291**, 899–911
7. Braiman, M.S., Mogi, T., Marti, T., Stern, L.J., Khorana, H.G., and Rothschild, K.J. (1988) Vibrational spectroscopy of bacteriorhodopsin mutants: light-driven proton transport involves protonation changes of aspartic acid residues 85, 96, and 212. *Biochemistry* **27**, 8516–8520
8. Mogi, T., Stern, L.J., Marti, T., Chao, B.H., and Khorana, H.G. (1988) Aspartic acid substitutions affect proton translocation by bacteriorhodopsin. *Proc. Natl. Acad. Sci. USA* **85**, 4148–4152
9. Otto, H., Marti, T., Holz, M., Mogi, T., Lindau, M., Khorana, H.G., and Heyn, M.P. (1989) Aspartic acid-96 is the internal proton donor in the reprotonation of the Schiff base of bacteriorhodopsin. *Proc. Natl Acad. Sci. USA* **86**, 9228–9232
10. Brown, L.S., Sasaki, J., Kandori, H., Maeda, A., Needleman, R., and Lanyi, J.K. (1995) Glutamic acid 204 is the terminal proton release group at the extracellular surface of bacteriorhodopsin. *J. Biol. Chem.* **270**, 27122–27126
11. Mitaku, S., Ikuta, K., Itoh, H., Kataoka, R., Naka, M., Yamada, M., and Suwa, M. (1988) Denaturation of bacteriorhodopsin by organic solvents. *Biophys. Chem.* **30**, 69–79
12. Mitaku, S., Suzuki, K., Odashima, S., Ikuta, K., Suwa, M., Kukita, F., Ishikawa, M., and Itoh, H. (1995) Interaction stabilizing tertiary structure of bacteriorhodopsin studied by denaturation experiments. *Proteins* **22**, 350–362
13. Lanyi, J.K. and Schobert, B. (2003) Mechanism of proton transport in bacteriorhodopsin from crystallographic structures of the K, L, M1, M2, and M2' intermediates of the photocycle. *J. Mol. Biol.* **328**, 439–450
14. Edman, K., Royant, A., Larsson, G., Jacobson, F., Taylor, T., van der Spoel, D., Landau, E.M., Pebay-Peyroula, E., and Neutze, R. (2004) Deformation of helix C in the low temperature L-intermediate of bacteriorhodopsin. *J. Biol. Chem.* **279**, 2147–2158
15. Takeda, K., Matsui, Y., Kamiya, N., Adachi, S., Okumura, H., and Kouyama, T. (2004) Crystal structure of the M intermediate of bacteriorhodopsin: allosteric structural changes mediated by sliding movement of a transmembrane helix. *J. Mol. Biol.* **341**, 1023–1037
16. Etoh, A., Itoh, H., and Mitaku, S. (1997) Light-induced denaturation of bacteriorhodopsin just above melting point of two-dimensional crystal. *J. Phys. Soc. Jpn.* **66**, 975–978
17. Dancsházy, Z., Tokaji, Z., and Dér, A. (1999) Bleaching of bacteriorhodopsin by continuous light. *FEBS Lett.* **450**, 154–157
18. Yokoyama, Y., Sonoyama, M., and Mitaku, S. (2002) Irreversible photobleaching of bacteriorhodopsin in a high-temperature intermediate state. *J. Biochem.* **131**, 785–790
19. Yokoyama, Y., Sonoyama, M., and Mitaku, S. (2004) Inhomogeneous stability of bacteriorhodopsin in purple membrane against photobleaching at high temperature. *Proteins* **54**, 442–454
20. Sonoyama, M., Yokoyama, Y., Taira, K., and Mitaku, S. (1999) Structural stability of bacteriorhodopsin at alkaline pH. *J. Biosci.* **24**, 67
21. Mukai, Y., Kamo, N., and Mitaku, S. (1999) Light-induced denaturation of bacteriorhodopsin solubilized by octyl-β-glucoside. *Protein Eng.* **12**, 755–759
22. Sasaki, T., Sonoyama, M., Demura, M., and Mitaku, S. (2005) Photobleaching of bacteriorhodopsin solubilized with Triton X-100. *Photochem. Photobiol.* **81**, 1131–1137
23. Wang, J.-P. and El-Sayed, M.A. (1999) Temperature jump-induced secondary structural change of the membrane protein bacteriorhodopsin in the premelting temperature region: a nanosecond time-resolved Fourier transform infrared study. *Biophys. J.* **76**, 2777–2783
24. Wang, J.-P. and El-Sayed, M.A. (2000) The effect of protein conformation change from α_{II} to α_{I} on the bacteriorhodopsin photocycle. *Biophys. J.* **78**, 2031–2036
25. Sonoyama, M. and Mitaku, S. (2004) High-temperature intermediate state of bacteriorhodopsin prior to the premelting transition of purple membrane revealed by reactivity with hydrolysis reagent hydroxylamine. *J. Phys. Chem. B* **108**, 19496–19500
26. Sonoyama, M., Hasegawa, T., Nakano, T., and Mitaku, S. (2004) Isomerization of retinal chromophore and conformational changes in membrane protein bacteriorhodopsin by solubilization with a mild non-ionic detergent, *n*-octyl-β-glucoside: an FT-Raman and FT-IR spectroscopic study. *Vib. Spectrosc.* **35**, 115–119

27. Brouillette, C.G., Muccio, D.D., and Finney, T.K. (1987) pH dependence of bacteriorhodopsin thermal unfolding. *Biochemistry* **26**, 7431–7438
28. Oesterhelt, D. and Stoeckenius, W. (1974) Isolation of the cell membrane of *Halobacterium halobium* and its fractionation into red and purple membrane. *Methods Enzymol.* **31**, 667–678
29. Rehorek, M. and Heyn, M.P. (1979) Binding of *all-trans*-retinal to the purple membrane. Evidence for cooperativity and determination of the extinction coefficient. *Biochemistry* **18**, 4977–4983
30. Kauppinen, J.K., Moffatt, D.J., Mantsch, H.H., and Cameron, D.G. (1981) Fourier self-deconvolution: a method for resolving intrinsically overlapped bands. *Appl. Spectrosc.* **35**, 271–276
31. Cladera, J., Sabés, M., and Padrós, E. (1992) Fourier transform infrared analysis of bacteriorhodopsin secondary structure. *Biochemistry* **31**, 12363–12368
32. Schulte, A., Bradley, II, L., and Williams, C. (1995) Equilibrium composition of retinal isomers in dark-adapted bacteriorhodopsin and effect of high pressure probed by near-infrared Raman spectroscopy. *Appl. Spectrosc.* **49**, 80–83
33. Schulte, A. and Bradley, L,II. (1995) High-pressure near-infrared Raman spectroscopy of bacteriorhodopsin light to dark adaptation. *Biophys. J.* **69**, 1554–1562
34. Rothschild, K.J. and Clark, N.A. (1979) Anomalous amide I infrared absorption of purple membrane. *Science* **204**, 311–312
35. Rothschild, K.J. and Clark, N.A. (1979) Polarized infrared spectroscopy of oriented purple membrane. *Biophys. J.* **25**, 473–487
36. Krimm, S. and Dwivedi, A.M. (1982) Infrared spectrum of the purple membrane: clue to a proton conduction mechanism? *Science* **216**, 407–408
37. Byler, D.M. and Susi, H. (1986) Examination of the secondary structure of proteins by deconvolved FTIR spectra. *Biopolymers* **25**, 469–487
38. Surewicz, W.K. and Mantsch, H.H. (1988) New insight into protein secondary structure from resolution-enhanced infrared spectra. *Biochim. Biophys. Acta* **952**, 115–130
39. Jackson, M., Haris, P.I., and Chapman, D. (1989) Fourier transform infrared spectroscopic studies of lipids, polypeptides and proteins. *J. Mol. Struct.* **214**, 329–355
40. Dong, A., Huang, P., and Caughey, W.S. (1990) Protein secondary structures in water from second-derivative amide I infrared spectra. *Biochemistry* **29**, 3303–3308
41. Sawatzki, J., Fishcer, R., Scheer, H., and Siebert, F. (1990) Fourier-transform Raman spectroscopy applied to photobiological systems. *Proc. Natl Acad. Sci. USA* **87**, 5903–5906
42. Curry, B., Broek, A., Lugtenburg, J., and Mathies, R. (1982) Vibrational analysis of *all-trans* retinal. *J. Am. Chem. Soc.* **104**, 5274–5286
43. Curry, B., Palings, I., Broek, A., Pardoen, J.A., Mulder, P.P.J., Lugtenburg, J., and Mathies, R. (1984) Vibrational analysis of 13-*cis* retinal. *J. Phys. Chem.* **88**, 688–702
44. Smith, S.O., Braiman, M.S., Myers, A.B., Pardoen, J.A., Courtin, J.M.L., Winkel, C., Lugtenburg, J., and Mathies, R.A. (1987) Vibrational analysis of the *all-trans*-retinal chromophore in light-adapted bacteriorhodopsin. *J. Am. Chem. Soc.* **109**, 3108–3125
45. Smith, S.O., Pardoen, J.A., Lugtenburg, J., and Mathies, R.A. (1987) Vibrational analysis of the 13-*cis*-retinal chromophore in dark-adapted bacteriorhodopsin. *J. Phys. Chem.* **91**, 804–819
46. Oesterhelt, D., Meentzen, M., and Schuhmann, L. (1973) Reversible dissociation of the purple complex in bacteriorhodopsin and identification of 13-*cis* and *all-trans*-retinal as its chromophores. *Eur. J. Biochem.* **40**, 453–463
47. Muccio, D.D. and Cassim, J.Y. (1979) Interpretations of the effects of pH on the spectra of purple membrane. *J. Mol. Biol.* **135**, 595–609
48. Bauer, P.-J., Dencher, N.A., and Heyn, M.P. (1976) Evidence for chromophore-chromophore interactions in the purple membrane from reconstitution experiments of the chromophore-free membrane. *Biophys. Struct. Mech.* **2**, 79–92
49. Hiraki, K., Hamanaka, T., Mitsui, T., and Kito, Y. (1981) Phase transition of the purple membrane and the brown holo-membrane X-ray diffraction, circular dichroism spectrum and absorption spectrum studies. *Biochim. Biophys. Acta* **647**, 18–28
50. Becher, B. and Ebrey, T.G. (1976) Evidence for chromophore-chromophore (exciton) interaction in the purple membrane of *Halobacterium halobium*. *Biochem. Biophys. Res. Commun.* **69**, 1–6
51. Balashov, S.P., Imasheva, E.S., Govindjee, R., and Ebrey, T.G. (1996) Titration of aspartate-85 in bacteriorhodopsin: what it says about chromophore isomerization and proton release. *Biophys. J.* **70**, 473–481
52. Richter, H.-T., Brown, L.S., Needleman, R., and Lanyi, J.K. (1996) A linkage of the pKa's of asp-85 and glu-204 forms part of the reprotonation switch of bacteriorhodopsin. *Biochemistry* **35**, 4054–4062
53. Balashov, S.P. (2000) Protonation reactions and their coupling in bacteriorhodopsin. *Biochim. Biophys. Acta* **1460**, 75–94
54. Tanio, M., Inoue, S., Yokota, K., Seki, T., Tuzi, S., Needleman, R., Lanyi, J.K., Naito, A., and Saitô, H. (1999) Long-distance effects of site-directed mutations on backbone conformation in bacteriorhodopsin from solid state NMR of [1-^{13}C]Val-labeled proteins. *Biophys. J.* **77**, 431–442
55. Sanz, C., Lazarova, T., Sepulcre, F., González-Moreno, R., Bourdelande, J.-L., Querol, E., and Padrós, E. (1999) Opening the Schiff base moiety of bacteriorhodopsin by mutation of the four extracellular Glu side chains. *FEBS Lett.* **456**, 191–195
56. Druckmann, S., Ottolenghi, M., Pande, A., Pande, J., and Callender, R.H. (1982) Acid-base equilibrium of the Schiff base in bacteriorhodopsin. *Biochemistry* **21**, 4953–4959
57. Dencher, N.A. and Heyn, M.P. (1982) Preparation and properties of monomeric bacteriorhodopsin. *Methods Enzymol.* **88**, 5–10